Initiation and termination of intraseasonal oscillations in nonlinear Laplacian spectral analysis-based indices

Eniko Székely*, Dimitrios Giannakis and Andrew J. Majda

Department of Mathematics, Courant Institute of Mathematical Sciences

New York University, New York, USA

December 3, 2015

Abstract

We present a statistical analysis of the initiation and termination of boreal winter and boreal summer intraseasonal oscillations (ISOs). This study uses purely convection (infrared brightness temperature) data over a 23-year time interval from 1984–2006. The indices are constructed via the nonlinear Laplacian spectral analysis (NLSA) method and display high intermittency and non-Gaussian statistics. We first define primary, terminal, and circumnavigating events in the NLSA-based indices, and then examine their statistics over the two-dimensional phase space representation of the ISOs. Roughly one primary and one terminal event per year were detected for the Madden-Julian oscillation (MJO), and roughly 1.3 events per year for the boreal summer ISO. We find that 91% of the recovered full MJO events are circumnavigating and exhibit very little to no retrograde (westward) propagation. The Indian Ocean emerges as the most active region in terms of both the onset and decay of events, however relevant activity occurs over all phases, consistent with previous work.

AMS Classification: 62-07

Keywords: nonlinear Laplacian spectral analysis, Madden-Julian oscillation, tropical intraseasonal oscillations

* *Corresponding author*: Eniko Székely, Courant Institute of Mathematical Sciences, New York University, 251 Mercer St, New York, NY 10012, USA. Email: eszekely@cims.nyu.edu

1 Introduction

Intraseasonal oscillations (ISOs) are large-scale modes of tropical variability playing a key role in the global climate system through extratropical interactions and feedback [Lau and Waliser, 2011; Zhang, 2013]. The dominant boreal winter ISO is the well-known Madden-Julian oscillation (MJO) [Madden and Julian, 1971, 1972], a 30–90-day eastward-propagating pattern of convective activity with zonal wavenumber 1–4. The MJO most commonly initiates in the western Indian Ocean and propagates over the Maritime Continent into the western Pacific at a speed of approximately $5 \mathrm{ms}^{-1}$ [Zhang, 2005]. On the other hand, the dominant boreal summer ISO (BSISO) has a northeastward-propagating pattern that tends to initiate in the Indian Ocean and propagate towards India and southeastern Asia [Wang and Rui, 1990; Kikuchi *et al.*, 2012]. As BSISO propagates into the Indian monsoon region at a frequency of 30–60 days, it largely influences the monsoon's onset and active/break phases [Goswami, 2011].

Despite the strong impact that tropical modes of intraseasonal variability have on predictability [Waliser, 2011], global climate models (GCMs) still perform poorly in simulating the ISOs [Hung *et al.*, 2013]. Many theories have been proposed in the literature to explain key features of the ISOs, like onset, strength or decay with a strong emphasis on the MJO and lately increasingly on the BSISO. In particular, various studies have found links between MJO initiation and other atmospheric variables such as low-level heating and moisture anomalies [Hendon and Salby, 1994; Khouider and Majda, 2006], the organization of planetary-scale wind anomalies into a wavenumber-1 pattern [Straub, 2013], or diabatic heating and precipitation anomalies [Ling *et al.*, 2014]. Different precursor conditions, particularly low-level moisture anomalies, have been related to MJO termination [Stachnik *et al.*, 2015]. The strength of the MJO has been linked to the El Niño Southern oscillation (ENSO) [Zhang and Gottschalck, 2002; Hendon *et al.*, 2007]. Strong MJO activity is often observed during ENSO-neutral years, while weak or absent MJO activity is typically associated with strong El Niño or La Niña episodes. In the Pacific, strong MJO activity is often observed 6–12 months prior to the peaks of El Niño episodes, e.g., the strong 1996-1997 MJO preceding the strong 1997-1998 El Niño [Kessler, 2011].

In addition to theories explaining ISO features, there is also a need for indices that can estimate their strength for predictability purposes. ISOs are propagating patterns of large areas of either enhanced or suppressed convection accompanied by lower- and upper-level atmospheric circulation anomalies. Construction of ISO indices therefore typically takes into account convection and/or circulation data. Proxies most often used for convective activity are either cloudiness (outgoing longwave radiation (OLR) and brightness temperature (T_b)) or rainfall data. Circulation is most commonly represented by lower- and upper-level zonal winds, but also streamfunctions and velocity potential data. Many data-based indices have been proposed to describe ISO activity, mainly for the MJO [Wheeler and Hendon, 2004; Matthews, 2008; Straub, 2013; Kiladis *et al.*, 2014], but also for the BSISO [Lee *et al.*, 2013; Kikuchi *et al.*, 2012; Székely *et al.*, 2015]. The techniques range from spacetime filtering methods [Wheeler and Kiladis, 1999; Kiladis *et al.*, 2005; Kikuchi and Wang, 2010] to empirical orthogonal functions (EOFs) [Lo and Hendon, 2000; Maloney and Hartmann, 1998; Kessler, 2001; Wheeler and Hendon, 2004; Kikuchi *et al.*, 2012; Ventrice *et al.*, 2013; Kiladis *et al.*, 2014], as well as hybrid filtering–EOF approaches [Roundy and Schreck, 2009]. Among the multitude of indices, the real-time multivariate MJO (RMM) index [Wheeler and Hendon, 2004] is the most common measure of ISO activity used all year-round, both for boreal winter and boreal summer activity. RMM is a combined measure of the first two EOFs of bandpass-filtered, and equatorially averaged OLR and 200hPa and 850hPa zonal wind data. In spite of the normalization of both the cloudiness and circulation components, the index is mainly determined by the circulation component [Straub, 2013]. In particular, the bivariate correlation between full RMM and only zonal wind RMM is 0.99.

Recently, Székely *et al.* [2015] (hereafter, S15) developed MJO and BSISO indices based purely on convection data. These indices were constructed using the nonlinear Laplacian spectral analysis (NLSA) [Giannakis and Majda, 2012, 2013, 2014], an eigendecomposition technique for high-dimensional (spatiotemporal) data combining ideas from machine learning and Takens delay-coordinate maps of dynamical systems. Compared to traditional approaches such as EOF and extended EOF analysis, NLSA provides superior timescale separation with no preprocessing of the input data such as seasonal partitioning, equatorial averaging, and bandpass filtering. The output of NLSA consists of a hierarchy of temporal and spatiotemporal modes that exist at different timescales. On the intraseasonal scale, NLSA outputs two distinct pairs of eigenmodes for the dominant boreal winter and boreal summer ISOs [Székely *et al.*, 2015]. This feature has proven particularly useful in the spatiotemporal reconstructions which reflect the distinct propagating patterns of the ISOs, i.e., eastward propagation for MJO vs. northeastward propagation for BSISO.

S15 built indices for MJO and BSISO from the NLSA eigenfunction pairs active in boreal winter and boreal summer, respectively. In this paper, we extend that study to analyze the onset, decay, and circumnavigation of both the MJO and BSISO as represented by the NLSA indices. Having distinct indices for MJO and BSISO allows us to emphasize their differences in terms of initiation, termination and circumnavigation. We define primary and terminal events with respect to predefined thresholds, similarly to previous works based on EOFs [Matthews, 2008; Straub, 2013; Stachnik *et al.*, 2015]. Because the NLSA-based indices are less noisy and have heavier-tailed distributions than the EOF-based indices, we are able to choose significantly lower values for the thresholds. Therefore this allows to detect earlier the onset of an event while avoiding a premature termination. The climatology of primary and terminal events is similar to that presented in previous works [Matthews, 2008; Straub, 2013; Stachnik *et al.*, 2015], but there are many differences in the details of individual events, especially in terms of circumnavigation. The number of primary and terminal events detected is significantly smaller than in the case of RMM, for example, and most ISOs are circumnavigating events with approximately one event occurring each year.

The paper is organized as follows. Section 2 describes the infrared brightness temperature data used in the analysis. The MJO and BSISO indices constructed using NLSA eigenfunctions are presented in Sect. 3, followed by examples and a study of the climatology of primary, terminal and circumnavigating events for each of the ISOs. Section 4 presents a detailed comparison of the two indices and the differences in their features followed by a comparison with other state-of-the-art indices for ISO analysis. The paper ends with conclusions in Sect. 5.

2 Data

Satellite infrared brightness temperature (T_b) data from the Cloud Archive User Service (CLAUS) [Hodges *et al.*, 2000] is used to extract pure cloudiness ISO signals and build MJO and BSISO indices. The data covers a time period of 23 years from January 1, 1984 to June 30, 2006. In the tropics, positive (negative) T_b anomalies are associated with reduced (increased) cloudiness and are a good proxy for tropical convection. The data is sampled over the tropical belt from 15°S to 15°N with a resolution of 1° (in both longitude and latitude) generating 2D samples with $n_{\text{long}} = 360$ longitude and $n_{\text{lat}} = 31$ latitude gridpoints. Observations are collected at an interval of $\delta t = 6$h, producing a dataset with $s = 32{,}868$ samples over the 23 years of the CLAUS record.

3 NLSA-based ISO indices

Blending ideas from the qualitative analysis of dynamical systems [Broomhead and King, 1986; Sauer *et al.*, 1991] and spectral graph theory from machine learning [Belkin and Niyogi, 2003; Coifman and Lafon, 2006], nonlinear Laplacian spectral analysis (NLSA) [Giannakis and Majda, 2012, 2013, 2014] identifies temporal and spatiotemporal patterns of interest in high-dimensional time series. NLSA extracts a set of temporal modes (which can be thought of as nonlinear principal components) through the eigenfunctions of a Laplace-Beltrami operator tailored to the nonlinear geometry and dynamics of the data. These temporal modes form a hierarchy of patterns that exist at different timescales, including interannual signals (e.g., ENSO), the annual cycle and its harmonics, and intraseasonal and diurnal signals [Székely *et al.*, 2015; Tung *et al.*, 2014]. While in RMM the first three harmonics of the annual cycle and the interannual variability are removed prior to the analysis, NLSA requires no preprocessing of the input data. The fact that the input data are not subjected to bandpass filtering opens up the possibility to explore directly the relationship between intraseasonal modes and other important modes of tropical variability, such as ENSO and the diurnal cycle.

The core of NLSA consists of: 1) time-lagged embedding using the delay method [Sauer *et al.*, 1991], followed by 2) the calculation of a set of eigenfunctions using kernel methods from machine learning. While RMM uses the principal components (PCs) given by the eigenfunctions of the covariance operator, NLSA employs the eigenfunctions of a discrete diffusion operator. The eigenfunctions of this operator form a natural orthonormal basis set of functions on the nonlinear manifold sampled by the data, providing superior timescale separation [Berry *et al.*, 2013] than what is possible through linear methods. Such patterns carry low variance and may fail to be captured by variance-based algorithms, yet may play an important dynamical role [Aubry *et al.*, 1993; Giannakis and Majda, 2012]. A detailed description of the method, i.e., the construction of the kernel and the computation of the eigenfunctions of the diffusion operator, can be found in Giannakis and Majda [2012, 2013, 2014]. S15 used the CLAUS T_b infrared temperature data sampled every $\delta t = 3\text{h}$ to extract a hierarchy of signals at different timescales, from interannual to diurnal signals. Here, after performing analyses using two sampling intervals, $\delta t = 3\text{h}$ and $\delta t = 6\text{h}$, we found that the latter generated slightly cleaner ISO signals, i.e., the intraseasonal modes were less mixed with the diurnal cycle. Because our main focus in this work is the analysis of intraseasonal signals we use the CLAUS T_b dataset with the lower sampling interval, $\delta t = 6\text{h}$. We mention that in RMM the diurnal cycle does not pose a problem because the observations are sampled once a day.

Let $\phi_i = (\phi_{1i}, \ldots, \phi_{Si})^T$ be the eigenvectors of the diffusion operator constructed from the data, where S is the number of available observations/samples. Each eigenvector corresponds to one temporal mode of variability in the observations, i.e., in this case brightness temperature. Figure 1 shows the two pairs of intraseasonal modes for the boreal winter MJO (Fig. 1(a, b)) and the boreal summer BSISO (Fig. 1(c, d)). Their associated Laplace-Beltrami eigenfunctions from NLSA are the pairs $\{\phi_{10}, \phi_{11}\}$ and $\{\phi_{16}, \phi_{17}\}$, respectively. Following Kikuchi *et al.* [2012] we construct individual indices for MJO and BSISO from the eigenfunction amplitudes, i.e.,

$$\begin{aligned} r_t^{\text{MJO}} &= \sqrt{\phi_{10}^2(t) + \phi_{11}^2(t)}, \\ r_t^{\text{BSISO}} &= \sqrt{\phi_{16}^2(t) + \phi_{17}^2(t)}. \end{aligned} \tag{1}$$

Figure 1(e, f) shows time series of the NLSA-based and RMM indices. The NLSA MJO and BSISO indices display a strong seasonality, with MJO mainly active in December–May and BSISO in May–

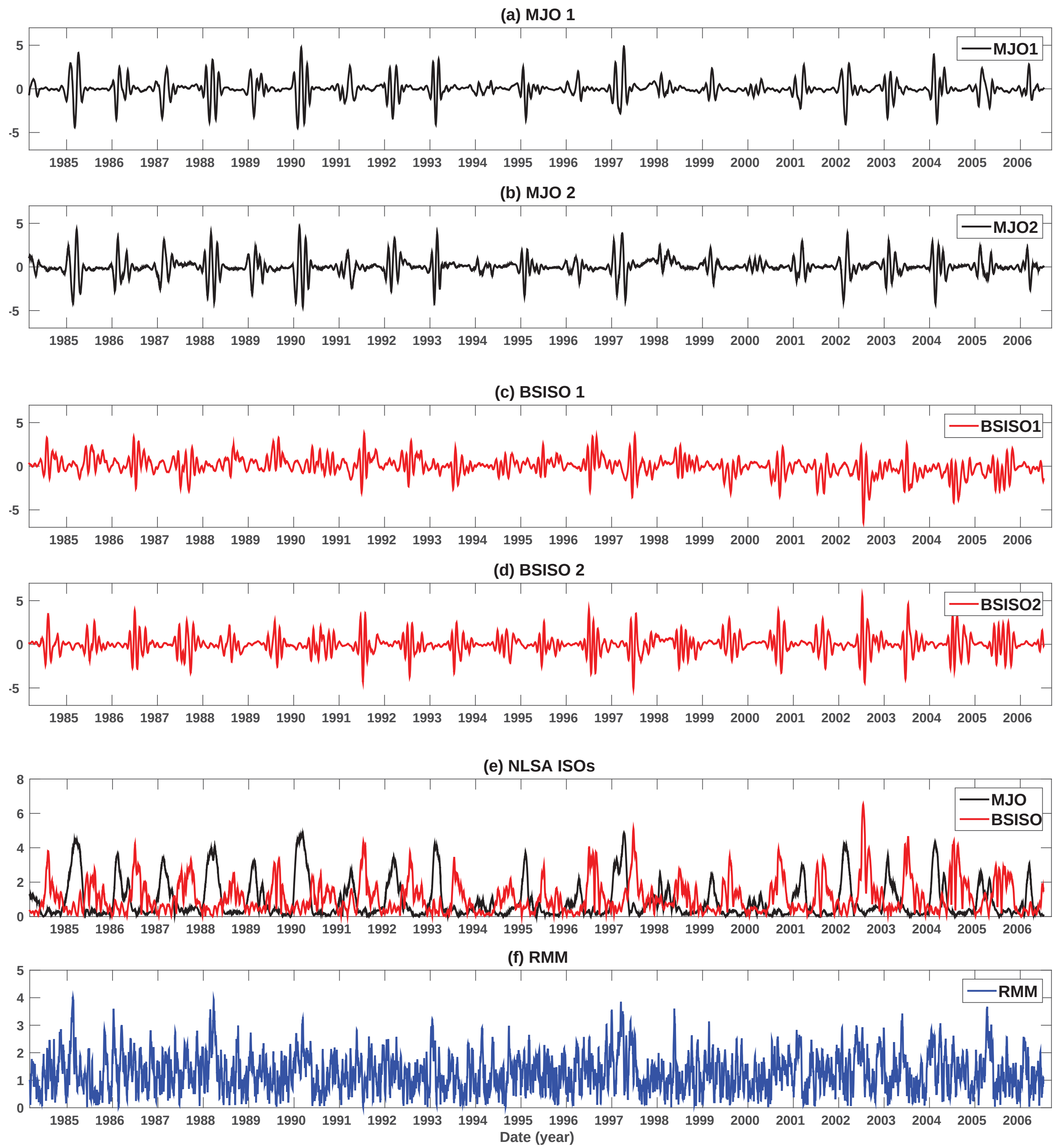

Figure 1: NLSA eigenfunctions for (a, b) boreal winter MJO, and (c, d) boreal summer BSISO; (e) NLSA-based indices r_t^{MJO} and r_t^{BSISO} from equation (1); (f) real-time multivariate MJO (RMM) index.

November. The RMM is active all-year round with the strongest activity taking place in December–May. In what follows we examine these NLSA indices in detail, focusing on the onset, decay and circumnavigation of ISO events and their statistics.

3.1 Madden-Julian oscillation

On the intraseasonal scale, the dominant mode of variability is the boreal winter MJO. The two-dimensional phase space diagram of the MJO eigenfunctions from NLSA is displayed in Fig. 2(a). This phase space is split into eight phases and its associated composite life cycle is reconstructed in Fig. 2(b). In this phase space, MJO follows a clockwise rotation that corresponds to an eastward propagation in the spatial domain.

Following previous works [Wheeler and Hendon, 2004; Straub, 2013; Stachnik *et al.*, 2015] we define full MJO events as strong persistent events (subject to the criteria described below) initiated and terminated by so-called primary and terminal events, respectively. First, similarly to Matthews [2008], Straub [2013], and Stachnik *et al.* [2015], we consider that *primary* events occur at the first day that the MJO index displays a magnitude greater than or equal to an initiation threshold r_P^{MJO}. Once an event initiates, it becomes a candidate for a full MJO as long as its amplitude does not decay below a given termination threshold r_T^{MJO}, called a *terminal* event. An event is considered a *full* MJO event if it fulfills the following three conditions with respect to the phase space diagram in Fig. 2(a): 1) has a clockwise rotation, i.e., eastward propagation, with 2) an amplitude greater than or equal to one standard deviation σ (here $\sigma = 1.06$), and 3) a propagation through at least four full phases in the phase space, i.e., a half cycle. The latter condition is similar to Straub [2013] and Stachnik *et al.* [2015], who require an MJO event to complete four phases of the RMM phase space in order to be considered "full". In Matthews [2008] a full MJO event was required to propagate through all eight phases of the RMM phase space, which is equivalent to a "circumnavigating" event in Straub [2013] and Stachnik *et al.* [2015].

Two examples of full MJOs for the winters of 1996–1997 and 2003–2004 are presented in Fig. 3. Both events were documented to be particularly strong. Strong MJOs have been observed prior to strong El Niño events, and this is the case of the 1996–1997 MJO [Kessler, 2011] which is considered to be a precursor for the initiation of the strong 1997–1998 El Niño. The second example depicts the strong MJO that has been observed in December 2003 – January 2004.[1] Figure 3(b) shows a rapid increase in amplitude starting on December 23, 2003 and a rapid decrease in amplitude after one full circumnavigation with the MJO reemerging and continuing until June, but at a lower intensity.

[1] http://www.esrl.noaa.gov/psd/mjo/MJOprimer/

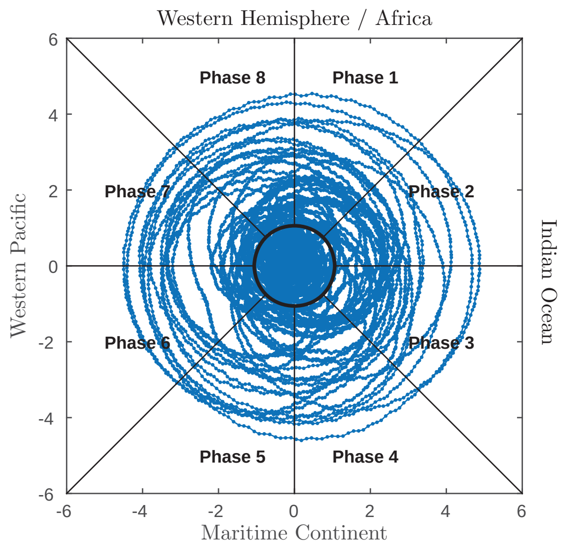

(a) MJO two-dimensional representation

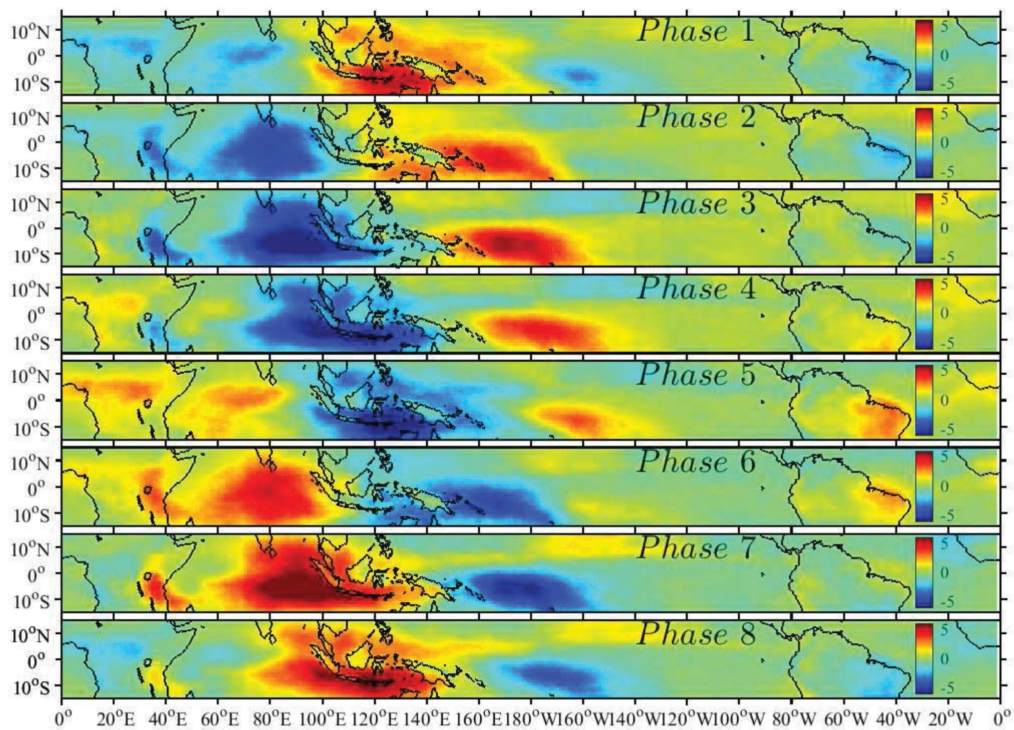

(b) MJO composite life cycle

Figure 2: (a) Two-dimensional phase space diagram for the MJO eigenfunctions from NLSA. The black circle denotes the constant amplitude of one standard deviation. (b) Spatiotemporal reconstructions of convective anomalies associated with each phase of the MJO index as depicted in (a).

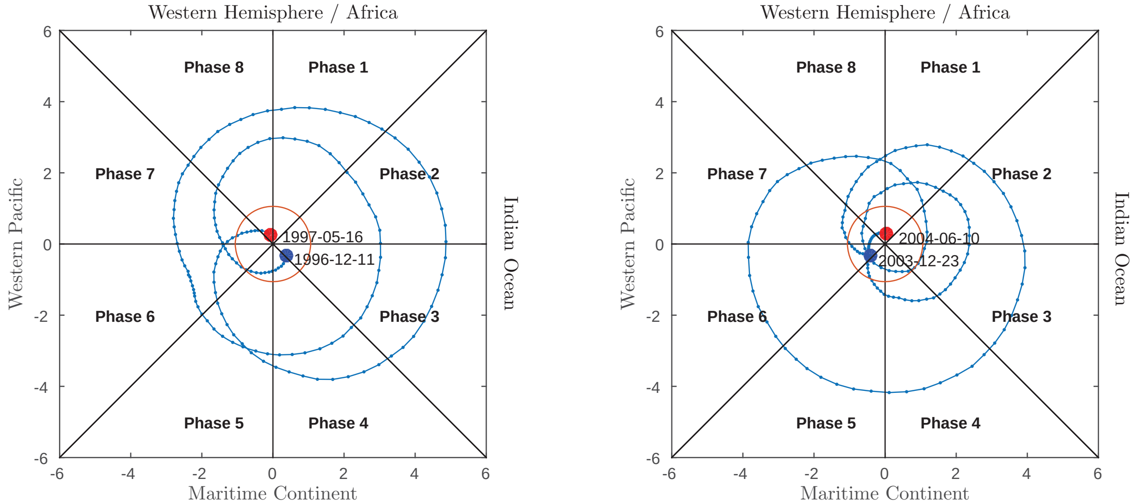

(a) 1996-1997 (b) 2003-2004

Figure 3: Examples of strong MJOs. (a) 1996–1997 [Kessler, 2011] and (b) 2003–2004.[1] The red-colored circle denotes the constant amplitude of one standard deviation. The 1996–1997 MJO event occurred prior to the strong 1997–1998 El Niño.

More specifically, a primary event occurs when the amplitude of the MJO index is lower than the initiation threshold r_P^{MJO} for three consecutive days, followed by an amplitude higher than r_P^{MJO} for two consecutive days. That is, we identify the time stamp t that satisfies the two conditions below:

$$r_{t+\tau}^{\mathrm{MJO}} < r_P^{\mathrm{MJO}}, \quad \tau = [-3 \;\; -2 \;\; -1] \text{ days},$$
$$r_{t+\tau}^{\mathrm{MJO}} \geq r_P^{\mathrm{MJO}}, \quad \tau = [0 \;\; 1 \;\; 2] \text{ days}.$$

The probability density function (PDF) for r_t^{MJO}, constructed via kernel density estimation, is plotted in Fig. 4. The PDF has a strong positive skewness, i.e., it carries large mass at high values of the index. We refer to the $r_t^{\mathrm{MJO}} = \sigma$ threshold as the stage where MJO enters the active phase. By visual inspection of the r_t^{MJO} time series (see Fig. 5 ahead), it appears that MJO initiates well in advance before reaching its active phase and therefore we choose the initiation threshold to be lower than the active phase threshold, here $r_P^{\mathrm{MJO}} = 0.5$ (Fig. 4). We performed robustness tests for the initiation threshold with values in the range $0.5 - 0.8$ and the climatology of primary events is relatively stable.

When an event has passed the active threshold, it can weaken in intensity, i.e., have an amplitude lower than the active amplitude threshold σ, without being considered to have terminated. This favors reemergence over the onset of a new primary event. An example is the 2003–2004 MJO in Fig. 3(b) where MJO weakens below the active threshold in Phase 3 and then reemerges after four phases, in Phase 8. We do not impose any constraints on the time that an event can stay below the active amplitude threshold

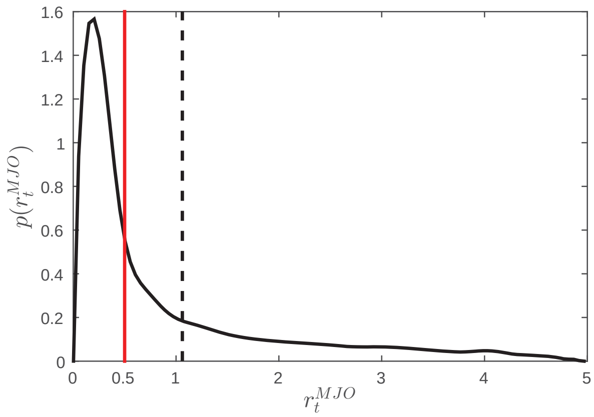

Figure 4: Probability density function of the NLSA-based MJO index. The red and black dashed vertical lines denote the threshold for initiation at $r_P^{\mathrm{MJO}} = 0.5$ and the threshold for active MJOs at one standard deviation $\sigma = 1.06$.

before regaining strength as long as it stays above the termination threshold r_T^{MJO} (Matthews [2008] and Straub [2013] call such events "successive" events, and Stachnik *et al.* [2015] call them "continuing" events). Here the termination threshold is $r_T^{\mathrm{MJO}} = 0.3$, chosen to be slightly lower than the initiation threshold $r_P^{\mathrm{MJO}} = 0.5$. When the MJO reaches the termination threshold, we call that event a terminal event. We performed robustness tests for the termination threshold with values in the range $0.3 - 0.6$ and the climatology of terminal events varies only slightly. Using the approach presented here, every primary event will have a terminal event associated to it.

Not all primary events develop into full MJO events. Over the 23 years of data there is a total of 36 primary events out of which only 27 go through at least four full phases in the phase space and are considered candidates for full MJOs. The 27 primary and their associated 27 terminal events are displayed in Fig. 5. Out of these 27 primary MJOs only 23 reach the amplitude threshold of one standard deviation and are considered full MJOs. Four primary events (1994, 1994, 2000, 2002) never attain the active amplitude threshold before terminating and therefore remain too weak all along to be considered active MJOs. Note that the choice of the threshold values is ad hoc and could discard weak but valid MJO events. An alternative approach would be to use multiple thresholds to classify an MJO into different categories, e.g., strong, medium or weak.

So far, we have discussed the question of *when* does the MJO initiate and terminate. In the following we will be looking at *where* does the MJO initiate and terminate? To answer this question we first need to estimate the statistics of primary and terminal events relative to the phases in Fig. 2(a) and determine the climatology of full MJO events. These statistics are summarized in Fig. 6 and Table

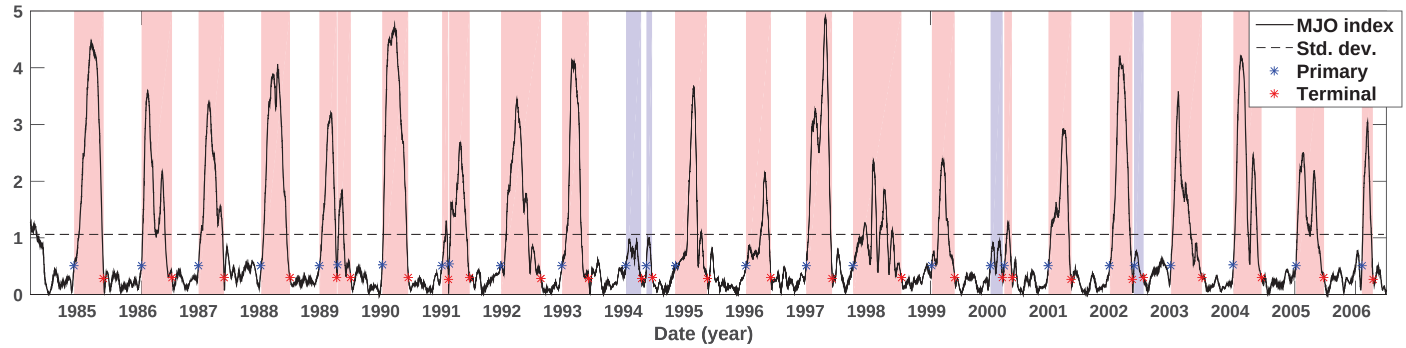

Figure 5: Time series of the NLSA-based MJO index r_t^{MJO}, showing a total of 23 full MJOs (red background). We identified a total of 36 primary and terminal events in the MJO index, but show here only the 27 events that go through at least four full phases in the phase space in Fig. 2(a). The nine events that are too short, i.e., less than half a cycle, are not shown. Out of these 27 events, 23 will reach the active threshold of one standard deviation and are therefore considered full MJOs (red background). Four of them (blue background) never reach the threshold of one standard deviation before terminating. We consider that these events never mature into an active MJO. Initiation and termination occur when the index reaches the thresholds of $r_P^{\mathrm{MJO}} = 0.5$ and $r_T^{\mathrm{MJO}} = 0.3$, respectively. The onset and decay of the MJOs is marked by primary (blue $\star$) and terminal (red $\star$) events.

Event type	NLSA MJO phase								
	1	2	3	4	5	6	7	8	
Primary (%)	9	13	17.5	17.5	4	13	13	13	100
Terminal (%)	17.5	22	13	9	4	4	17.5	13	100
Total (%)	13.25	17.5	15.25	13.25	4	8.5	15.25	13	100
Circumnavigating (%)	9.66	9.66	19	19	5	9.66	14	14	100

Table 1: Statistics of the 23 full MJO events for the time period from 1984–2006 for each MJO phase as identified through the NLSA-based MJO index. Results are shown in percentages. Circumnavigating events are a subset of primary events and do not count towards the total number of events per phase.

1. The primary and terminal events associated with full MJOs are relatively equidistributed among the phases, however we have observed some patterns that we detail in the following. In particular, the Indian Ocean (Phases 2 and 3) is the region with the highest frequency of occurrence of both primary and terminal events. During the 23-year observation period, a total of 7 primary events (3 events in Phase 2 and 4 events in Phase 3) and 8 terminal events (5 events in Phase 2 and 3 events in Phase 3) occurred in the Indian Ocean. This result is consistent with the observations, at least in terms of initiation, as MJO's main basin for onset is known to be the Indian Ocean. The next most frequent initiation happens in the Western Pacific (Phases 6 and 7) with a total of 6 primary events (3 events in Phase 6 and 3 events in Phase 7). Frequent termination is associated with the Western Hemisphere and Africa (Phases 8 and 1) with a total of 7 terminal events (3 events in Phase 8 and 4 events in Phase 1). Among more localized domains that witness frequent events is the Western Maritime Continent (Phase 4) with 4 primary events and 2 terminal events. The phase space diagrams for primary and terminal events, together with their trajectories after initiation and before termination, are shown in Figs. 12 and 13 of Appendix A. The index often travels a few full phases between initiation/termination and the active MJO threshold (one standard deviation), with less rapid transitions than in the case of RMM. A summary of the initiation/termination statistics for the RMM index is presented in Sect. 4.2.

Out of the 23 full MJOs, 21 are circumnavigating events, i.e., they go through at least one full cycle in the phase space, and many of them (15) actually circumnavigate the globe two or three times between onset and decay. The two events that do not complete a full cycle are the December 1990 – January 1991 event, prior to the 1991 MJO, and the spring-summer MJO of year 2000. The latter occurred after a weak MJO earlier that year and is associated with the strong La Niña event of year 2000 [Shabbar and Yu, 2009].

3.2 Boreal summer intraseasonal oscillation

The two-dimensional representation of the BSISO through the corresponding pair of NLSA eigenfunctions (Fig. 1(c, d)) is plotted in Fig. 7(a). The phase space is split into eight phases and its associated composite life cycle is reconstructed in Fig. 7(b). Note the difference in the propagating patterns of the MJO and BSISO. While MJO has a dominant eastward propagating pattern (Fig. 2(b)), BSISO propagates northeastward towards the Indian and Asian monsoon regions (Fig. 7(b)). Unlike the MJO, the BSISO eigenfunctions follow a counterclockwise rotation in the two-dimensional phase space.

Similarly to an MJO event, a full BSISO event is defined as: 1) a counterclockwise rotation corresponding to a northeastward propagation in the spatial domain, with 2) an amplitude greater than or equal to one standard deviation σ (here $\sigma = 0.94$), and 3) a propagation through at least four full

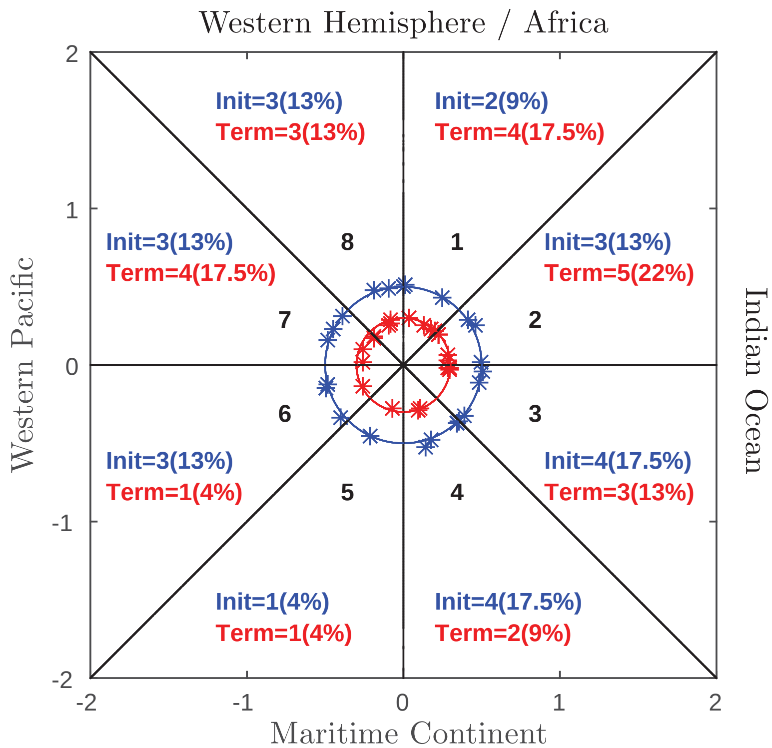

Figure 6: Frequency of primary and terminal events for each MJO phase associated with the 23 full MJOs that occurred between years 1984–2006. The initiation $r_P^{\text{MJO}} = 0.5$ and termination $r_T^{\text{MJO}} = 0.3$ thresholds are denoted with blue and red circles, respectively. The individual primary and terminal events are denoted with blue and red ($\star$).

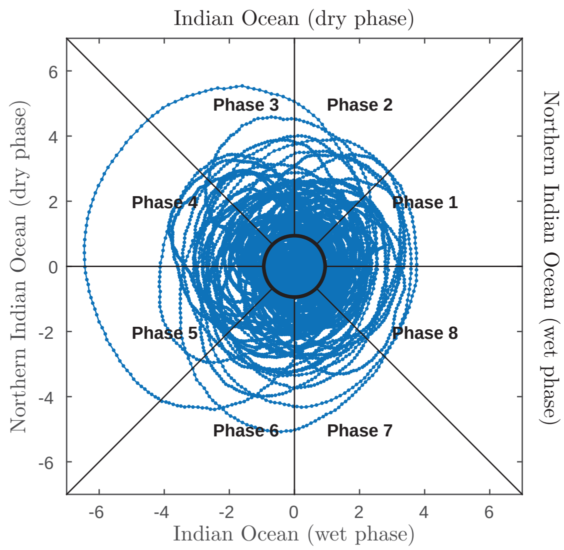

(a) BSISO two-dimensional representation

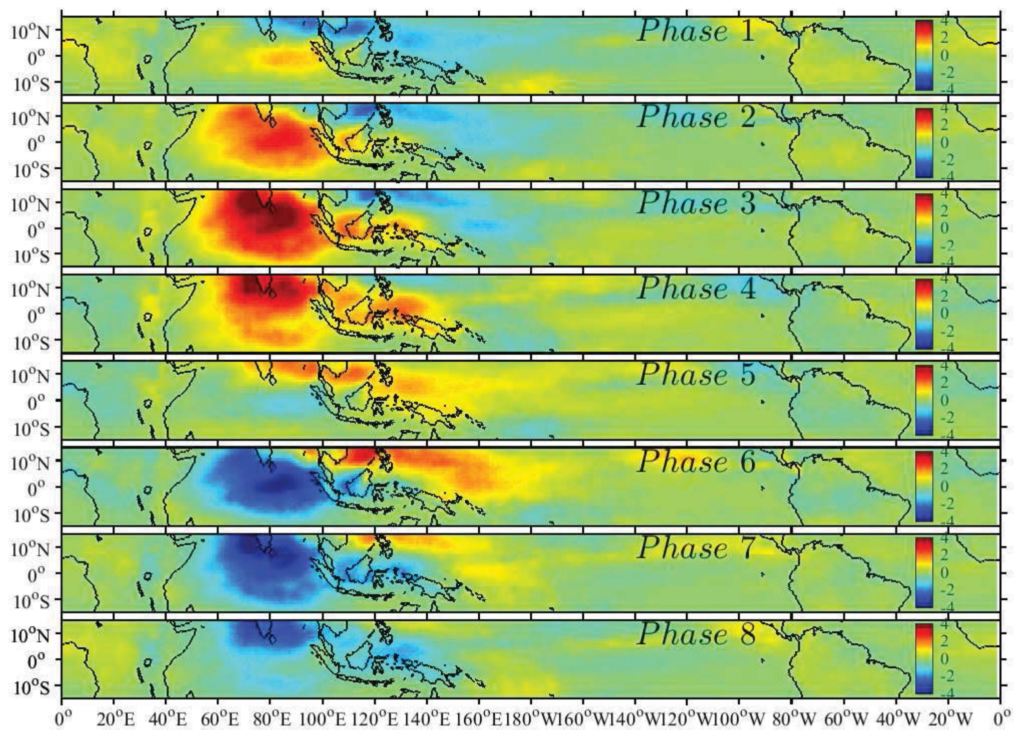

(b) BSISO composite life cycle

Figure 7: (a) Two-dimensional phase space diagram for the BSISO eigenfunctions from NLSA. The black circle denotes the constant amplitude of one standard deviation. (b) Spatiotemporal reconstructions of convective anomalies associated with each phase of the BSISO index as depicted in (a).

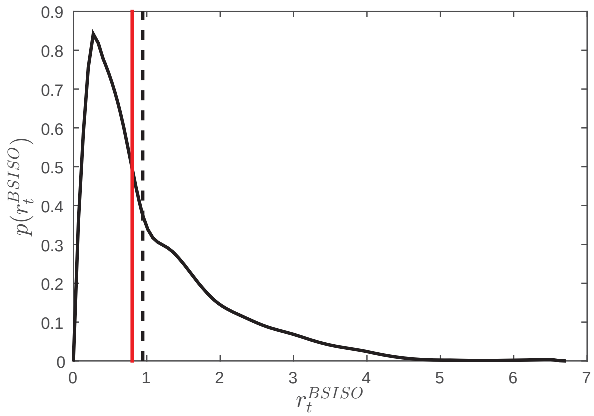

Figure 8: Probability density function of the NLSA-based BSISO index. The red and black dashed vertical lines denote the threshold for initiation at $r_P^{\text{BSISO}} = 0.8$ and the threshold for active BSISOs at one standard deviation $\sigma = 0.94$.

phases, i.e., a half cycle, in the phase space. Primary and terminal BSISO events are defined similarly to MJOs, but using different threshold values. Figure 8 shows the PDF of the BSISO index which is skewed, though significantly less than the PDF of the MJO index. To adapt to this feature of the BSISO index we choose slightly higher threshold values for initiation and termination. Specifically, we set the primary event onset to $r_P^{\text{BSISO}} = 0.8$ and the terminal event decay threshold to $r_T^{\text{BSISO}} = 0.6$. We have again chosen the termination threshold slightly lower than the initiation threshold to counter for local small fluctuations in the time series.

We identified a total of 79 primary and terminal events in the BSISO index between years 1984–2006, out of which only 31 events went through at least half a cycle in the phase space. All of the latter 31 events (Fig. 9) develop into full BSISOs as they all reach the active amplitude threshold of one standard deviation $\sigma = 0.94$. The frequency of primary and terminal events per phase is displayed in Fig. 10 and Table 2. The statistics for the BSISO initiation/termination are less equally distributed compared to the MJO. Specifically, the highest activity, both in terms of initiation and termination, is observed in the wet phase over the Indian Ocean (Phases 6 and 7) with a total of 23 events out of which 11 are primary events (7 events in Phase 6 and 4 events in Phase 7), and 12 are terminal events (5 events in Phase 6 and 7 events in Phase 7). Significant initiation also occurs in Phase 2 (the dry phase of BSISO over the Indian Ocean) with 10 primary events. Two localized domains that experience a high frequency of terminal events are Phase 8 with 7 events and Phase 4 with 5 events. Phase 8 can be associated with the final decay of the BSISO with no new event following, while Phase 4 can be associated with an event that terminates and is shortly followed by a new event, i.e., the start of a new dry phase in the Indian

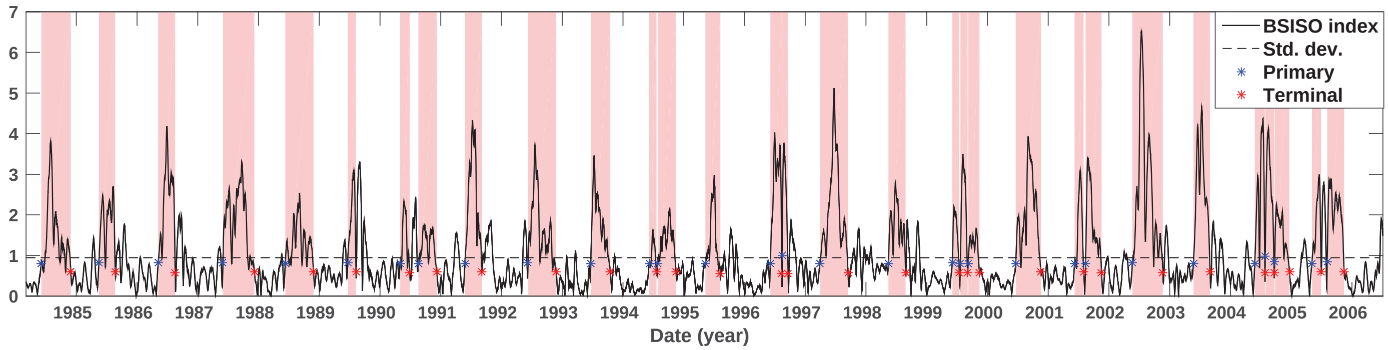

Figure 9: Time series of the NLSA-based BSISO index r_t^{BSISO}, showing a total of 31 full BSISOs (red background). We identified a total of 79 primary and terminal events in the BSISO index, but show here only the 31 events that go through at least four full phases in the phase space in Fig. 7(a). All these 31 events will reach the active threshold of one standard deviation and are therefore considered full BSISOs. Initiation and termination occur when the index reaches the thresholds of $r_P^{\mathrm{BSISO}} = 0.8$ and $r_T^{\mathrm{BSISO}} = 0.6$, respectively. The onset and decay of the BSISOs is marked by primary (blue $\star$) and terminal (red $\star$) events.

Event type	NLSA BSISO phase								
	1	2	3	4	5	6	7	8	
Primary (%)	13	32	6.5	3	3	23	13	6.5	100
Terminal (%)	3	6	10	16	3	16	23	23	100
Total (%)	8	19	8.25	9.5	3	19.5	18	14.75	100

Table 2: Statistics of the 31 full BSISO events for the time period from 1984–2006 for each BSISO phase as identified through the NLSA-based BSISO index. Results are shown in percentages.

Ocean. S15 observed that the BSISO tends to initiate with a dry phase over the eastern Indian Ocean, equivalent to Phase 2 in Fig. 7(b), with 32% of events initiating in this phase in Fig. 10.

4 Discussion

4.1 Comparison of MJO and BSISO statistics

Following Kikuchi *et al.* [2012] we build an ISO bimodal index (Fig. 11) using the amplitude of the individual MJO and BSISO indices ($r_t^{\mathrm{MJO}}, r_t^{\mathrm{BSISO}}$). An observation is considered significant, i.e., active event, if either the MJO or BSISO index is higher than or equal to one standard deviation. The NLSA-

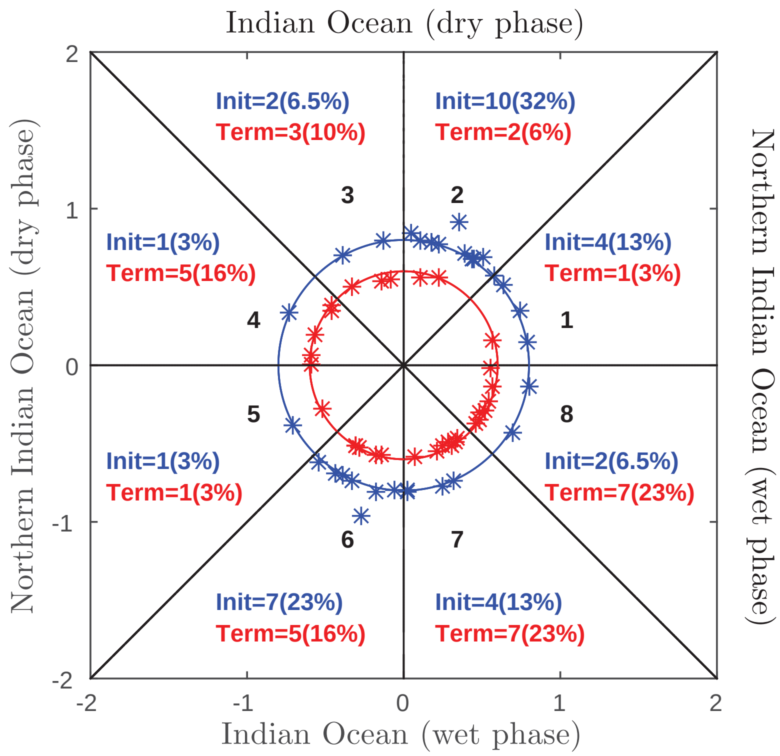

Figure 10: Frequency of primary and terminal events for each BSISO phase associated with the 31 full BSISOs that occurred between years 1984–2006. The initiation $r_P^{\mathrm{BSISO}} = 0.8$ and termination $r_T^{\mathrm{BSISO}} = 0.6$ thresholds are denoted with blue and red circles, respectively. The individual primary and terminal events are denoted with blue and red ($\star$).

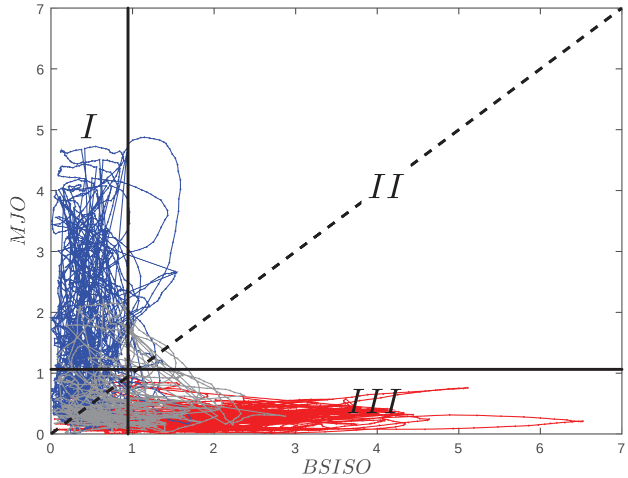

Figure 11: NLSA-based ISO bimodal index ($r_t^{\text{MJO}}, r_t^{\text{BSISO}}$). Following Kikuchi *et al.* [2012], three periods are plotted in different colors: June–October (red), December–April (blue), and otherwise (gray). The solid lines indicate the threshold for significant ISO events corresponding to one standard deviation of the MJO and BSISO indices. Observations are classified into three categories according to their associated regions as follows: I) MJO events, III) BSISO events, II) MJO or BSISO events. The majority of significant ISO events are either MJO events (I) occurring in December–April, or BSISO events (II) occurring in June–October.

based bimodal index has high discriminating power, i.e., the majority of events are either active MJOs or active BSISOs. Moreover, the active MJO and BSISO events are correctly assigned to the boreal winter and boreal summer, respectively. S15 compared the nonlinear NLSA ISO bimodal index with a linear ISO bimodal index based on the singular spectrum analysis (SSA, [Ghil *et al.*, 2002]), and observed a significantly higher classification power for NLSA compared to SSA. According to the analysis in Stachnik *et al.* [2015], the difference between the climatology of MJO events for year-round vs. boreal winter is only 1-2 %. In our case, such a comparison is not necessary since the NLSA-based MJO and BSISO modes have strong seasonal activity in the boreal winter and boreal summer, respectively.

The number of primary and terminal events and their distribution per phase depends on the threshold values used for initiation and termination. The active threshold value (here one standard deviation) has a direct impact on the number of full ISOs detected. More importantly, these values affect the *when* and *where* of each individual event's initiation and termination. As the transitions between phases are smooth, even small changes in the threshold values will affect the initiation/termination phase assigned to each primary/terminal event. The index often travels through two or three phases between initiation (e.g., for MJO at $r_P^{\text{MJO}} = 0.5$), and the active threshold of one standard deviation. Our robustness tests confirmed that a unique threshold value for all primary and terminal events does not impact significantly the statistics. However, from a prediction standpoint, it has a strong influence on the identification of individual events.

4.2 Comparison with other indices

In previous works [Matthews, 2008; Straub, 2013; Stachnik *et al.*, 2015] the climatology of primary, terminal and circumnavigating MJO events has been analyzed through the lens of the RMM index [Wheeler and Hendon, 2004], a combined measure of cloudiness and upper- and lower-level zonal winds. RMM uses latitudinal averaging over the tropical belt 15°S–15°N and therefore captures mainly the zonal component of equatorially symmetric patterns, i.e., the eastward propagation characteristic of the MJO. The spatial patterns associated with the first principal components of the RMM index are reconstructed separately for boreal winter (December–January–February) and boreal summer (May–June). The weakening of the eastward-propagating signal during boreal summer allows the spatial reconstructions to recover the BSISO-specific northeastward-propagating pattern, however to a significantly lesser extent than possible through NLSA reconstructions.

The statistics of primary MJO events have been mainly presented in Matthews [2008] and Straub [2013], and of terminal events in Stachnik *et al.* [2015], using the RMM index. Straub [2013] performed multiple analyses using only OLR, only wind, or both OLR and wind, and observed that the OLR contributes minimal information to the RMM index. The individual events identified using these different data sources differed significantly in their distribution over the phases, i.e., the same event initiated in different phases when using different data sources. During the 32-year time interval from 1979–2010, a total of 28 primary events was detected in the RMM index (both cloudiness and circulation) and a slightly lower number of primary events in the cloudiness-only (27 events) or circulation-only (23 events) index. Stachnik *et al.* [2015] identified a total of 154 primary and 154 terminal events in the RMM index, despite working with approximately the same time interval as Straub [2013], that is, 1979–2012 *vs.* 1979–2010. The large discrepancy between the number of events identified via the two analyses seems to be a consequence of the details used in the implementation of the event selection algorithms. While Straub [2013] used a length of 7 days as a requirement for continuous eastward propagation and amplitude value for consecutive days, Stachnik *et al.* [2015] used a more relaxed requirement of 3 days. Here, we used a requirement of 3 days prior and 2 days after initiation and obtained a frequency of events closer to the results presented in Straub [2013] where the requirement was of 7 days.

Overall, the higher number of events identified via RMM compared to NLSA is due to the reduced intermittency and the higher number of rapid transitions that traverse the threshold value of one standard deviation. Our results on MJO statistics are consistent with previous research [Matthews, 2008; Straub, 2013; Stachnik *et al.*, 2015] in that the onset and decay can occur in any phase of the MJO phase space. The boreal summer ISO statistics have been considered so far only as part of the year-round statistics of the RMM index, but no separate analysis via a stand-alone BSISO index has been performed previously.

5 Conclusion

In this paper, we have presented a statistical analysis of intraseasonal oscillation events using recently proposed indices [Székely *et al.*, 2015] for the boreal winter and boreal summer ISOs that are based on the nonlinear Laplacian spectral analysis (NLSA) method. Following previous studies [Matthews, 2008; Straub, 2013; Stachnik *et al.*, 2015] we defined primary, terminal and circumnavigating events relative to these new indices. While ISO events have been largely studied through the lens of the year-round active RMM index, here we performed two separate analyses for the boreal winter and boreal summer ISOs. This is the first study considering the climatology of the BSISO as a standalone phenomenon with its unique northeastward propagating pattern. Its importance stems from its strong impact on the Indian and southasian monsoon's onset and active/break phases [Goswami, 2011].

While RMM combines the convection and circulation components of the atmosphere into one index, the NLSA indices are extracted from pure convection data without preprocessing (in particular, without seasonal partitioning, bandpass filtering, or zonal averaging). Straub [2013] shows that the cloudiness component of the data contributes only little new information to the RMM index compared to the circulation component. Nevertheless, we have seen throughout this paper that using purely infrared brightness temperature data we are able to recover the dominant spatiotemporal patterns associated with the boreal winter and boreal summer ISOs through distinct families of NLSA eigenfunctions.

We found that 91% of the MJOs identified for the period 1984–2006 were circumnavigating events with one or multiple circumnavigations. Also, the NLSA MJO index has very little to no retrograde (westward) propagation. Over the 23 years of observation from 1984–2006 we found 23 full MJO events (roughly 1 event per year). Our definition of the primary and terminal events favored reemergence over the decay of an event and the onset of a new primary event. We imposed no constraints over the time that an ISO could stay below the active threshold value as long as it was not decaying below a termination threshold. For BSISO, we found a higher frequency of primary and terminal events with roughly 3.5 events per year, however only 40% of these events developed into full BSISOs (roughly 1.3 events per year).

Both MJO and BSISO exhibit strong activity in the Indian Ocean, with the centers of convection moving eastward and northeastward, respectively. The Indian Ocean is well acknowledged in previous studies and observations to be the main basin for MJO initiation. Additionally, in this study we showed that the Indian Ocean plays an important role in BSISO initiation, with 38.5% of primary events initiating in Phases 2 and 3. The Indian Ocean also witnesses significant termination for both MJO and BSISO, with 35% of MJOs decaying in this region, and 39% of BSISOs terminating during the wet phase over the Indian Ocean (Phases 6 and 7). An alternative scenario worth considering is to study ISO initiation conditional on a given region (e.g., Indian Ocean) with more relaxed constraints on the amplitude of the index. Straub [2013] also considered this scenario by stating that by the time the RMM index reaches the initiation threshold of one standard deviation, the MJO might in fact have already initiated. This question requires further analysis such as the existence of precursors for initiation/termination (similar to Stachnik *et al.* [2015]) other than just the magnitude of the MJO index, which we plan to pursue in future work.

Acknowledgements

The research of Andrew J. Majda and Dimitrios Giannakis is partially supported by ONR MURI grant 25-74200-F7112. Eniko Székely is supported as a postdoctoral fellow through this grant.

A Primary and terminal MJO events

In this appendix we plot the primary and terminal events identified in the NLSA-based MJO index together with their trajectories. For primary events we display the trajectories after the initiation of an MJO at $r_P^{\text{MJO}} = 0.5$ for the ensuing 30 days. It is important to note that in most cases the transition of the index between phases happens slowly, with a few exceptions, e.g., the 1986-01-01, 1989-03-24 events, where the transition from the initiation threshold to one standard deviation occurs in the same phase. For terminal events we display the trajectories 30 days prior to termination. The transitions between phases from one standard deviation to termination at $r_T^{\text{MJO}} = 0.3$ are smooth, however slightly more rapid transitions are seen than at initiation. We emphasize that, due to the smooth transitions between phases, the choice of the threshold values for initiation and termination do play a role in the identification of the onset and decay of each event, even if they do not influence significantly the statistics presented in Figs. 6 and 10 and Tables 1 and 2. As mentioned in Sect. 5, one possible scenario is that all ISOs initiate in (or near) the same region, such as the Indian Ocean, but at different intensities (amplitudes).

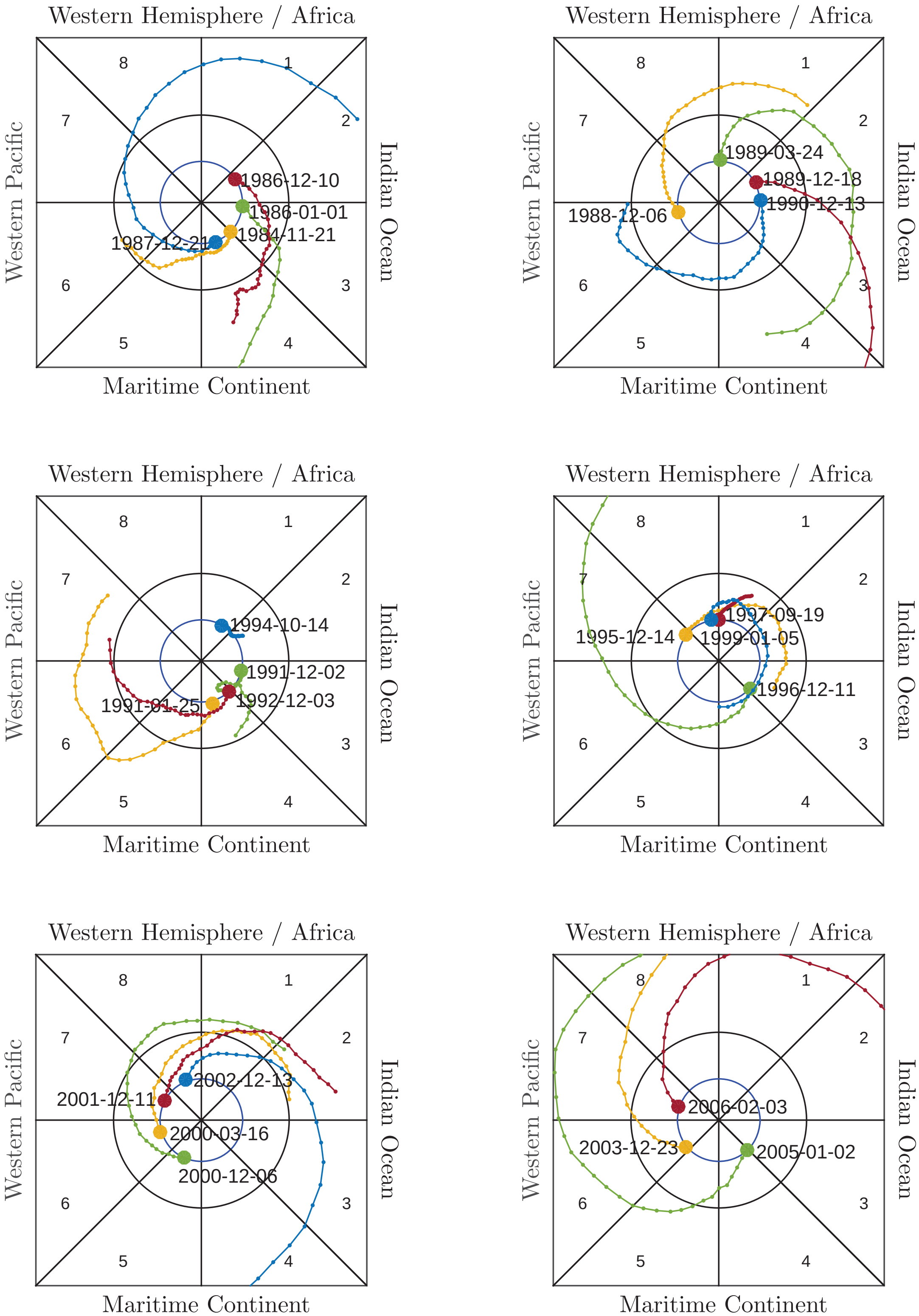

Figure 12: Primary events associated with full MJOs and their trajectory for the ensuing 30 days. The trajectories often show a slow increase in amplitude between initiation at $r_P^{\mathrm{MJO}} = 0.5$ and one standard deviation. The index often travels between one and three full phases between these two values.

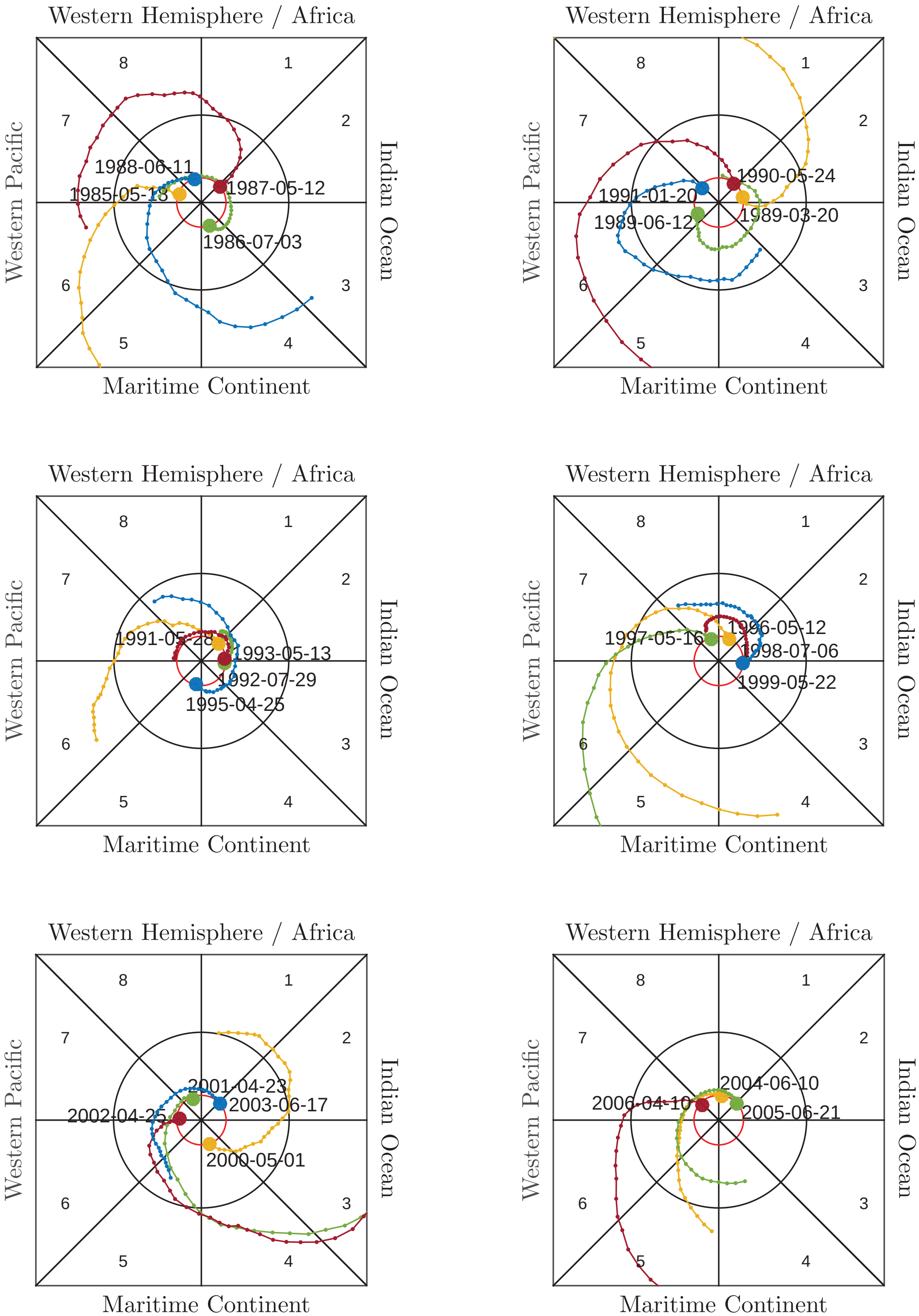

Figure 13: Terminal events associated with full MJOs and their trajectory 30 days in advance. The trajectories often show a slow decrease in amplitude between one standard deviation and termination at $r_T^{\text{MJO}} = 0.3$. The index often travels between one and three full phases between these two values.

References

Aubry, N., Lian, W.-Y., and Titi, E. S. (1993). Preserving symmetries in the proper orthogonal decomposition. *SIAM J. Sci. Comput.*, **14**, 483–505.

Belkin, M. and Niyogi, P. (2003). Laplacian eigenmaps for dimensionality reduction and data representation. *Neural Comput.*, **15**, 1373–1396.

Berry, T., Cressman, R., Greguric Ferencek, Z., and Sauer, T. (2013). Time-scale separation from diffusion-mapped delay coordinates. *SIAM J. Appl. Dyn. Sys.*, **12**, 618–649.

Broomhead, D. S. and King, G. P. (1986). Extracting qualitative dynamics from experimental data. *Phys. D*, **20**(2–3), 217–236.

Coifman, R. R. and Lafon, S. (2006). Diffusion maps. *Appl. Comput. Harmon. Anal.*, **21**, 5–30.

Ghil, M. *et al.* (2002). Advanced spectral methods for climatic time series. *Rev. Geophys.*, **40**.

Giannakis, D. and Majda, A. J. (2012). Nonlinear Laplacian spectral analysis for time series with intermittency and low-frequency variability. *Proc. Natl. Acad. Sci.*, **109**(7), 2222–2227.

Giannakis, D. and Majda, A. J. (2013). Nonlinear Laplacian spectral analysis: Capturing intermittent and low-frequency spatiotemporal patterns in high-dimensional data. *Stat. Anal. Data Min.*, **6**(3), 180–194.

Giannakis, D. and Majda, A. J. (2014). Data-driven methods for dynamical systems: Quantifying predictability and extracting spatiotemporal patterns. In R. Melnik, editor, *Mathematical and Computational Modeling: With Applications in Engineering and the Natural and Social Sciences*, page 288. Wiley, Hoboken.

Goswami, B. N. (2011). South Asian monsoon. In W. Lau and D. Waliser, editors, *Intraseasonal Variability of the Atmosphere-Ocean Climate System*, pages 21–64.

Hendon, H. H. and Salby, M. L. (1994). The life cycle of the Madden-Julian oscillation. *Journal of the Atmospheric Sciences*, **51**(15), 2225–2237.

Hendon, H. H., Wheeler, M. C., and Zhang, C. (2007). Seasonal dependence of the MJO–ENSO relationship. *J. Climate*, **20**, 531–543.

Hodges, K., Chappell, D., Robinson, G., and Yang, G. (2000). An improved algorithm for generating global window brightness temperatures from multiple satellite infra-red imagery. *J. Atmos. Oceanic Technol.*, **17**, 1296–1312.

Hung, M.-P., Lin, J.-L., Wang, W., Kim, D., Shinoda, D., and Weaver, S. J. (2013). MJO and convectively coupled equatorial waves simulated by CMIP5 climate models. *J. Climate*, **26**, 6185–6214.

Kessler, W. (2011). The oceans. In W. K. Lau and D. E. Waliser, editors, *Intraseasonal Variability in the Atmosphere-Ocean Climate System*, pages 199–236. Springer.

Kessler, W. S. (2001). EOF representations of the Madden-Julian Oscillation and its connection with ENSO. *J. Climate*, **14**, 3055–3061.

Khouider, B. and Majda, A. (2006). A simple multicloud parameterization for convectively coupled tropical waves. part I: Linear analysis. *Journal of the Atmospheric Sciences*, **63**, 1308–1323.

Kikuchi, K. and Wang, B. (2010). Spatiotemporal wavelet transform and the multiscale behavior of the Madden-Julian oscillation. *J. Climate*, **23**, 3814–3834.

Kikuchi, K., Wang, B., and Kajikawa, Y. (2012). Bimodal representation of the tropical intraseasonal oscillation. *Climate Dyn.*, **38**, 1989–2000.

Kiladis, G. N., Straub, K. H., and T., H. P. (2005). Zonal and vertical structure of the Madden-Julian oscillation. *J. Atmos. Sci.*, **62**, 2790–2809.

Kiladis, G. N., Dias, J., Straub, K. H., Wheeler, M. C., Tulich, S. N., Kikuchi, K., Weickmann, K. M., and Ventrice, M. J. (2014). A comparison of OLR and circulation-based indices for tracking the MJO. *Mon. Wea. Rev.*, **142**, 1697–1715.

Lau, W. K. M. and Waliser, D. E. (2011). *Intraseasonal Variability in the Atmosphere–Ocean Climate System*. Springer-Verlag, Berlin.

Lee, J.-Y., Wang, B., Wheeler, M., Xiouhua, F., Waliser, D., and Kang, I.-S. (2013). Real-time multivariate indices for the boreal summer intraseasonal oscillation over the Asian summer monsoon region. *Climate Dynamics*, **40**, 493–509.

Ling, J., Li, C., Zhou, W., and Jia, X. (2014). To begin or not to begin? A case study on the MJO initiation problem. *Theoretical and Applied Climatology*, **115**(1-2), 231–241.

Lo, F. and Hendon, H. (2000). Empirical extended-range prediction of the Madden-Julian oscillation. *Mon. Wea. Rev.*, **128**.

Madden, R. A. and Julian, P. R. (1971). Detection of a 40–50 day oscillation in the zonal wind in the tropical Pacific. *J. Atmos. Sci.*, **28**(5).

Madden, R. A. and Julian, P. R. (1972). Description of global-scale circulation cells in the tropics with a 40–50 day period. *J. Atmos. Sci.*, **29**(6), 1109–1123.

Maloney, E. D. and Hartmann, D. L. (1998). Frictional moisture convergence in a composite life cycle of the Madden-Julian oscillation. *J. Climate*, **11**, 2387–2403.

Matthews, A. J. (2008). Primary and successive events in the MaddenJulian oscillation. *Quarterly Journal of the Royal Meteorological Society*, **134**(631), 439–453.

Roundy, P. E. and Schreck, C. J. I. (2009). A combined wavenumberfrequency and time-extended EOF approach for tracking the progress of modes of large-scale organized tropical convection. *Q. J. R. Meteorol. Soc.*, **135**, 161–173.

Sauer, T., Yorke, J. A., and Casdagli, M. (1991). Embedology. *J. Stat. Phys.*, **65**(3–4), 579–616.

Shabbar, A. and Yu, B. (2009). The 19982000 la nia in the context of historically strong la nia events. *Journal of Geophysical Research: Atmospheres*, **114**(D13).

Stachnik, J., Waliser, D., and Majda, A. J. (2015). Precursor environmental conditions associated with the termination of MaddenJulian oscillation events. *J. Atmos. Sci.*, **72**, 19081931.

Straub, K. H. (2013). MJO initiation in the real-time multivariate MJO index. *J. Climate*, **26**, 1130–1151.

Székely, E., Giannakis, D., and Majda, A. J. (2015). Extraction and predictability of coherent intraseasonal signals in infrared brightness temperature data. *Climate Dyn.*

Tung, W.-w., Giannakis, D., and Majda, A. J. (2014). Symmetric and antisymmetric signals in MJO deep convection. Part I: Basic modes in infrared brightness temperature. *J. Atmos. Sci.*, **71**, 3302–3326.

Ventrice, M. Wheeler, M., Hendon, H., Schreck, C., Thorncroft, C., and Kiladis, G. (2013). A modified multivariate Madden-Julian oscillation index using velocity potential. *Mon. Wea. Rev.*, **141**(12), 4197–4210.

Waliser, D. (2011). Predictability and forecasting. In W. K. Lau and D. E. Waliser, editors, *Intraseasonal Variability in the Atmosphere-Ocean Climate System*, pages 433–468. Springer.

Wang, B. and Rui, H. (1990). Synoptic climatology of transient tropical intraseasonal convection a nomalies: 1975–1985. *Meteor. Atmos. Phys.*, **44**, 43–61.

Wheeler, M. and Kiladis, G. N. (1999). Convectively coupled equatorial waves: Analysis of clouds and temperature in the wavenumber-frequency domain. *J. Atmos. Sci.*, **56**(3), 374–399.

Wheeler, M. C. and Hendon, H. H. (2004). An all-season real-time multivariate MJO index: Development of an index for monitoring and prediction. *Mon. Wea. Rev.*, **132**(8), 1917–1932.

Zhang, C. (2005). The Madden-Julian oscillation. *Rev. Geophys.*, **43**, RG2003.

Zhang, C. (2013). Madden-Julian oscillation: bridging weather and climate. *Bull. Amer. Meteor. Soc.*, **94**, 1849–1870.

Zhang, C. and Gottschalck, J. (2002). SST anomalies of ENSO and the Madden-Julian oscillation in the equatorial Pacific. *Journal of Climate*, **15**, 2429–2445.